Journal of Molecular Structure 1119 (2016) 188–199

Contents lists available at ScienceDirect

Journal of Molecular Structure

journal homepage: http://www.elsevier.com/locate/molstruc

Spectroscopic, quantum chemical studies, Fukui functions, *in vitro* antiviral activity and molecular docking of 5-chloro-*N*-(3-nitrophenyl) pyrazine-2-carboxamide

S.H. Rosline Sebastian [a, b], Monirah A. Al-Alshaikh [c], Ali A. El-Emam [d], C. Yohannan Panicker [e, *], Jan Zitko [f], Martin Dolezal [f], C. VanAlsenoy [g]

[a] Department of Physics, Karpagam University, Eachanari, Coimbatore, Tamilnadu, India
[b] Christhu Jyothi Public School, Rajakkad, Idukki, Kerala, India
[c] Department of Chemistry, College of Sciences, King Saud University, Riyadh, 11451, Saudi Arabia
[d] Department of Pharmaceutical Chemistry, College of Pharmacy, King Saud University, Riyadh, 11451, Saudi Arabia
[e] Department of Physics, Fatima Mata National College, Kollam, Kerala, India
[f] Faculty of Pharmacy in Hradec Kralove, Charles University in Prague, Heyrovskeho 1203, Hradec Kralove, 500 05, Czech Republic
[g] Department of Chemistry, University of Antwerp, Groenenborgerlaan 171, B-2020, Antwerp, Belgium

ARTICLE INFO

Article history:
Received 8 February 2016
Received in revised form
1 April 2016
Accepted 25 April 2016
Available online 28 April 2016

Keywords:
DFT
Antiviral activity
Cytotoxicity
Pyrazine
Spectroscopic
Molecular docking

ABSTRACT

The molecular structural parameters and vibrational frequencies of 5-chloro-*N*-(3-nitrophenyl)pyrazine-2-carboxamide have been obtained using density functional theory technique in the B3LYP approximation and CC-pVDZ (5D, 7F) basis set. Detailed vibrational assignments of observed FT-IR and FT-Raman bands have been proposed on the basis of potential energy distribution and most of the modes have wavenumbers in the expected range. In the present case, the NH stretching mode is a doublet in the IR spectrum with a difference of 138 cm^{-1} and is red shifted by 76 cm^{-1} from the computed value, which indicates the weakening of NH bond resulting in proton transfer to the neighboring oxygen atom. The molecular electrostatic potential has been mapped for predicting sites and relative reactivities towards electrophilic and nucleophilic attack. The hyperpolarizability values are calculated in order to find its role in nonlinear optics. From the molecular docking study, amino acids Asn161, His162 forms H-bond with pyrazine ring and Trp184, Gln19 shows H-bond with C=O group and the docked ligand, title compound forms a stable complex with cathepsin K and the results suggest that the compound might exhibit inhibitory activity against cathepsin K. Moderate *in vitro* antiviral activity with EC_{50} at tens of μM was detected against feline herpes virus, coxsackie virus B4, and influenza A/H1N1 and A/H3N2.

1. Introduction

The pyrazine moiety is an important part of many clinically used drugs, including anticancer, diuretic [1], antidiabetic, antithrombotic, antidepressants or anti-infective (antituberculotics, bactericides and fungicides) agents and offers many possibilities in drug development [2–4]. Some *N*-phenylpyrazine-2-carboxamides with various substituents both on the pyrazine and phenyl core were described to possess significant antimycobacterial activity [5]. Pyrazinamide, a nicotinamide analogue, plays an important role in TB-therapy [6] and has multiple mechanisms of action and as a prodrug it is metabolized via mycobacterial enzyme pyrazinamidase to form pyrazinoic acid [7]. Pyrazinoic acid accumulates intracellularly and lowers pH in mycobacterial cell, which leads to inhibition of membrane transport and depletion of energy [8]. Derivatives of heterocyclic compounds such as pyridazine, pyrimidine, and pyrazine are valuable chemotherapeutic agents [4,6]. The pyrazine ring is present in a number of naturally occurring compounds in the forms of pteridines and antibiotics. Pyrazine-2-caboxamides was recognized as the first line antimycobacterial agent exhibiting a promising antibacterial and antifungal activity. Pyrazine-2-carboxamide may be used in the treatment of multidrug resistant tuberculosis, a major growing problem among HIV-infected patients [9]. The title compound of 5-chloro-*N*-(3-nitrophenyl)pyrazine-2-carboxamide was shown to possess

* Corresponding author.
E-mail address: cyphyp@rediffmail.com (C.Y. Panicker).

http://dx.doi.org/10.1016/j.molstruc.2016.04.088
0022-2860/

in vitro whole cell antimycobacterial activity against *M. tuerculosis* H37Rv with minimum inhibitory concentration of 3.13 μg/mL (11 μM). Several pyrazine derivatives proved to be clinically significant antiviral drugs. For examples, flutimide [10] and its analogues [11] are potent and species selective inhibitors of influenza virus endonuclease. Active metabolite (ribofuranosyltriphosphate) of favipiravir (T-705) is an inhibitor of RNA-dependent RNA polymerase, effective against RNA viruses [12]. Telaprevir is a serine protease inhibitor used in the treatment of hepatitis C [13]. The presence of pyrazine-2-carboxamide motif in favipiravir and telaprevir led us to examine the antiviral activity of the title compound, which itself is an *N*-substituted pyrazine-2-carboxamide.

2. Experimental

2.1. Synthesis of 5-chloro-N-(3-nitrophenyl)pyrazine-2-carboxamide

The title compound was prepared as described previously [14] by convenient two-step synthesis using 5-hydroxypyrazine-2-carboxylic acid (5-hydroxy-POA; Sigma-Aldrich, Darmstadt, Germany) as a starting compound. The 5-chloro-*N*-(3-nitrophenyl) pyrazine-2-carboxamide was obtained as white solid in 67% yield (after all purification steps). The identity and purity of the compound was checked by melting point (223.5–225.1 °C; 224.5–225.6 °C) in literature [14] and ^{1}H and ^{13}C NMR spectra.

2.2. Spectra measurement

The FT-IR spectrum (Fig. 1) was recorded using KBr pellets on a DR/Jasco FT-IR 6300 spectrometer in KBr pellets with a spectral resolution of 4 cm^{-1}. The FT-Raman spectrum (Fig. 2) was obtained on a Bruker RFS 100/s, Germany. For excitation of the spectrum the emission of a Nd:YAG laser was used, excitation wavelength 1064 nm, maximal power 150 mW, measurement of solid sample. One thousand scans were accumulated with a total registration time of about 30 min. The spectral resolution after apodization was 2 cm^{-1}. NMR spectra were recorded on Varian VNMR S500 (Varian, Palo Alto, CA, USA) at 500 MHz for ^{1}H and 125 MHz for ^{13}C. The spectra were recorded in DMSO-d_6 at ambient temperature. The chemical shifts as δ values in parts per million (ppm) are indirectly referenced to tetramethylsilane (TMS) *via* the solvent signal (see Scheme 1).

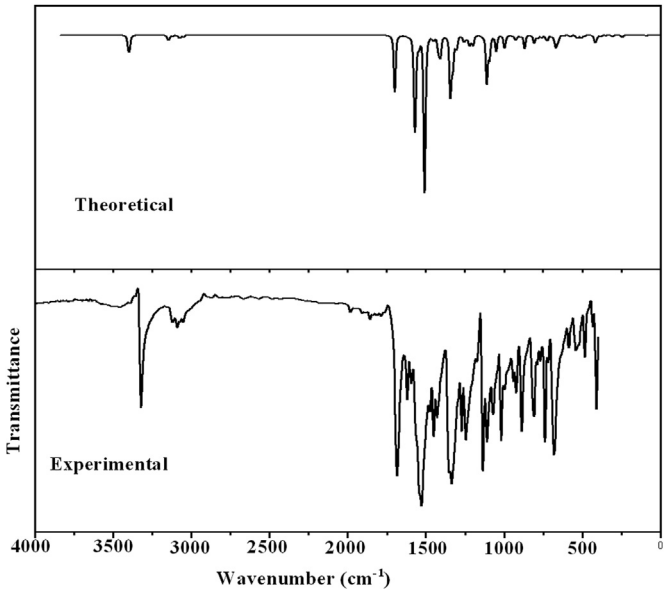

Fig. 1. FT-IR spectrum of 5-chloro-*N*-(3-nitrophenyl)pyrazine-2-carboxamide.

2.3. Antiviral evaluation

Antiviral activity in cell culture was assessed by cytopathic effect (CPE) reduction assays using a broad panel of viruses [15,16]. To perform the tests, the virus was added to semiconfluent cell cultures in 96-well plates and, simultaneously, serial dilutions of the test compound were added. The plates were incubated until clear CPE was reached (typically 3–6 days). The antiviral activity was expressed as EC_{50}, which is the effective concentration causing 50% reduction of CPE compared non-treated infected cells. The CPE was evaluated by visual microscopy and/or by standard colorimetric formazan-based MTS cell viability assay. Viruses examined on Crandell-Rees Feline Kidney (CRFK) cells are: feline coronal virus and feline herpes virus. Viruses examined on human embryonic lung fibroblast (HEL) cells are: herpes simplex virus type 1 (HSV-1), a thymidine kinase-deficient (TK) HSV-1 KOS strain resistant to acyclovir, herpes simplex virus type 2 (HSV-2), vaccinia virus, human adenoviurs type 2 and vesicular stomatitis virus (VSV). Viruses examined on human cervix carcinoma (HeLa) cells are: VSV, Coxsackie B4 virus and respiratory syncytial virus (RSV). Viruses examined on African Green Monkey (Vero) cells are: parainfluenza-3 virus, reovirus-1, Sindbis virus, Coxsackie B4 virus and Punta Toro virus. Viruses examined on Madin-Darby canne kidney (MDCK) cells: human influenza A/H1N1, A/H3N2 and B viruses. Finally, activity against human immunodeficiency virus (HIV) type 1 and type 2 was studied in human MT-4 lymphoblast cells.

Unless stated otherwise, the tested strains and cell for cultivation were obtained from the American Type Culture Collection (ATCC). The strain A/HK/7/87 (A/H3N2) was obtained from J. Neyts (Katholieke Universiteit Leuven, Leuven, Belgium).

2.4. Evaluation of in vitro cytotoxicity

Compound's cytotoxic activity was measure as a control test of the cell viability during the antiviral screening assays. Cytotoxicity was determined in uninfected cells, which were incubated with serial compound dilutions for 72 h. CC_{50}, that is compound concentration producing 50% cytotoxic effect, was determined by colorimetric formazan-based MTS assay. Alternatively, the toxicity was expressed as minimal cytotoxic concentration (MCC), which represented the tested compound concentration causing minimal changes in cell morphology as detected microscopically.

3. Computational details

Calculations of the title compound were carried out with the Gaussian09 program [17] using B3LYP/CC-pVDZ (5D, 7F) basis set to predict the molecular structure and frequencies and a scaling factor of 0.9613 had to be used for obtaining a considerably better agreement with experimental data [18]. The hybrid B3LYP functional is a combination of the Becke's three parameter exchange functional [19] and Lee-Yang-Parr correlation functional [20,21]. The cc-pVDZ basis sets have had redundant functions removed and have been rotated in order to increase computational efficiency [22]. Structural parameters corresponding to the optimized geometry of the title compound (Fig. 3) are given in Table 1. The assignments of the calculated frequencies are done using Gaussview [23] and GAR2PED [24] software. With respect to the carboxamide moiety, C10–O25–N11–H24 two different conformations are possible AI and BII (Fig. 4). The energies of the conformation AI are −1321.94142319 a.u. and that of BII is −1321.95789451 a.u. The

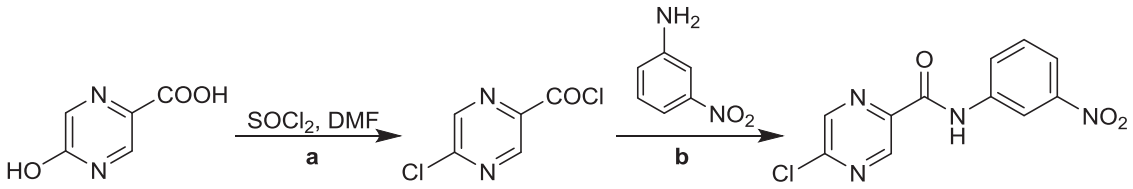

Scheme 1. Synthesis of 5-chloro-*N*-(3-nitrophenyl)pyrazine-2-carboxamides. Conditions: (a) anhydrous toluene, 90 °C, 1 h; (b) anhydrous acetone, TEA, RT.

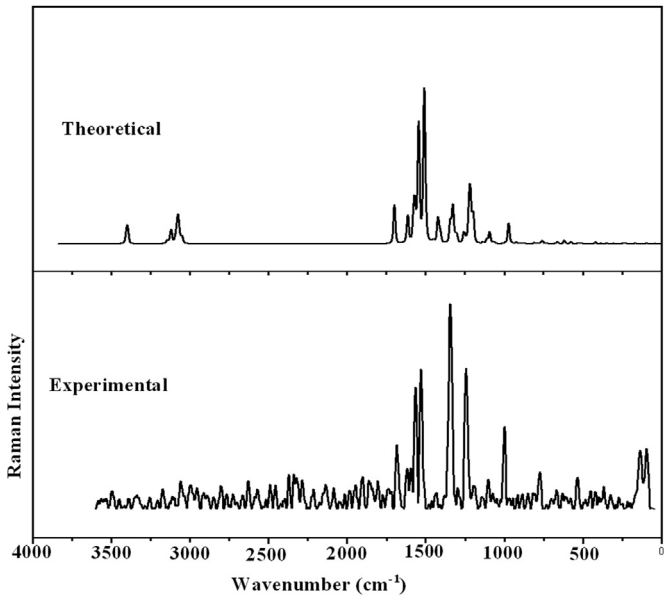

Fig. 2. FT-Raman spectrum of 5-chloro-*N*-(3-nitrophenyl)pyrazine-2-carboxamide.

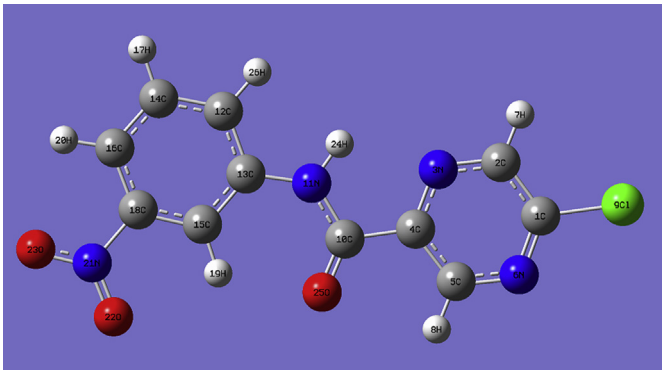

Fig. 3. Optimized geometry of 5-chloro-*N*-(3-nitrophenyl)pyrazine-2-carboxamide.

least energy is for BII and this conformation is taken for the further theoretical calculations in the article.

4. Results and discussion

In the following discussion the phenyl and pyrazine rings are designated as Ph and Pz.

4.1. Geometrical parameters

The C–C bond lengths in the phenyl ring lie in the range 1.3930–1.4083 Å and for benzene the C–C bond length is 1.3993 Å [25] and for benzaldehyde 1.3973 Å [26]. In the present case, the bond lengths C_4–C_{10}, C_{10}–O_{25}, C_{10}–N_{11}, C_{13}–N_{11} are 1.5081, 1.2235, 1.3706, 1.4027 Å and the corresponding reported values are 1.5248, 1.2486, 1.3521, 1.4109 Å [27]. For the title compound, the pyrazine bond lengths, C_4–C_5, C_5–N_6, C_1–N_6, C_1–C_2, C_2–N_3 and C_4–N_3 are 1.3991, 1.3401, 1.3222, 1.4058, 1.3303 Å and the corresponding reported values are 1.3955, 1.3482, 1.3521, 1.4109, 1.3532, 1.3477 [27]. The C–N bond lengths in the pyrazine ring of the title compound are much shorter than the normal C–N sing bond that is referred to 1.49 Å [27] and the same results are shown for the two C–C bonds lengths in the pyrazine ring and are also smaller than that of the normal C–C single bond of 1.54 Å [28]. The bond lengths C_{10}–N_{11} = 1.3706 and C_{13}–N_{11} = 1.4027 Å are also shorter than the normal C–N single bond of 1.49 Å, which confirms this bond to have some character of a double or conjugated bond [29].

For the title compound C=O bond length is 1.2235 Å and the corresponding reported values are 1.2253 Å [30], 1.2486 Å [27] and 1.2253 Å [31] and according to literature [32,33] the changes in bond lengths in C=O and C–N are consistent with the following interpretation: that is, hydrogen bond decreases the double bond character of C=O bond and increases the double bond character of C–N bond. For the title compound the N–O bond lengths are 1.2236 and 1.2257 Å which was in agreement with the reported values 1.2245 and 1.2237 Å [34]. The C–N–O angles are reported as 117.7 and 117.5° [34] whereas for the title compound, the angles are 117.3 and 117.7°.

At N_{11} position, the angles C_{13}–N_{11}–H_{24} is 117.5, C_{10}–N_{11}–H_{24} is 113.8 and C_{13}–N_{11}–C_{10} is 128.7°. This asymmetry of angles at N_{11} position indicates the weakening of N_{11}–H_{24} bond resulting in proton transfer to the oxygen atom O_{25} [35]. At C_4 position the angles C_5–C_4–N_3 is increased by 1.4° and N_3–C_4–C_{10} is reduced by 1.1° from 120° and this asymmetry reveals the interaction between the amide moiety and the pyrazine ring. At C_{10} position, the bond angles are C_4–C_{10}–N_{11} = 112.8°, C_4–C_{10}–O_{25} = 121.1° and N_{11}–C_{10}–O_{25} = 126.1° and this asymmetry gives the interaction between carbonyl group and the neighbouring pyrazine ring.

4.2. IR and Raman spectra

The observed IR, Raman bands, calculated (scaled) frequencies and assignments are given in Table 2.

4.2.1. NO_2 modes

Nitro benzene shows NO_2 stretching modes in the region 1535 ± 30 and 1345 ± 30 cm^{-1} [36] in the present case bands observed at 1566, 1345 cm^{-1} in the IR spectrum, 1565, 1345 cm^{-1} in the Raman spectrum and 1568, 1342 cm^{-1} theoretically as assigned as NO_2 stretching modes [36]. Both the NO_2 stretching modes, 1568, 1342 cm^{-1} are IR and Raman active with IRintensities, 361.12, 270.96 and Raman activities, 178.80, 120.14 and have PEDs 54 and 83%. In aromatic compounds the deformation modes of NO_2 are assigned at 850 ± 60, 740 ± 50 and 540 ± 70 cm^{-1} [36]. For the title compound, bands observed at 811, 724, 526 cm^{-1} (IR), 810, 730, 530 cm^{-1} (Raman) and 808, 726, 528 cm^{-1} are assigned as NO_2 deformation modes. According to the calculations, the deformation modes of NO_2 are IR active with IR intensities, 26.99, 29.49 and

Table 1
Optimized geometrical parameters of 5-chloro-*N*-(3-nitrophenyl)pyrazine-2-carboxamide.

Bond lengths (Å)					
C1–C2	1.4058	C1–N6	1.3222	C1–Cl9	1.7508
C2–N3	1.3303	C2–H7	1.0921	N3–C4	1.3443
C4–C5	1.3991	C4–C10	1.5081	C5–N6	1.3401
C5–H8	1.0915	C10–N11	1.3706	C10–O25	1.2235
N11–C13	1.4027	N11–H24	1.0181	C12–C13	1.4083
C12–C14	1.3939	C12–H26	1.0932	C13–C15	1.4045
C14–C16	1.3961	C14–H17	1.0914	C15–C18	1.393
C15–H19	1.0858	C16–C18	1.3936	C16–H20	1.088
C18–N21	1.4844	N21–O22	1.2236	N21–O23	1.2257
Bond angles (°)					
C2–C1–N6	123.3	C2–C1–Cl9	118.9	N6–C1–Cl9	117.9
C1–C2–N3	120.3	C1–C2–H7	121.3	N3–C2–H7	118.4
C2–N3–C4	117.4	N3–C4–C5	121.4	N3–C4–C10	118.9
C5–C4–C10	119.7	C4–C5–N6	121.6	C4–C5–H8	120.3
N6–C5–H8	118.0	C1–N6–C5	116.2	C4–C10–N11	112.8
C4–C10–O25	121.1	N11–C10–O25	126.1	C10–N11–C13	128.7
C10–N11–H24	113.8	C13–N11–H24	117.5	C13–C12–C14	120.8
C13–C12–H26	119.4	C14–C12–H26	119.8	N11–C13–C12	117.7
N11–C13–C15	122.9	C12–C13–C15	119.5	C12–C14–C16	120.5
C12–C14–H17	119.6	C16–C14–H17	119.9	C13–C15–C18	118.0
C13–C15–H19	121.3	C18–C15–H19	120.6	C14–C16–C18	117.7
C14–C16–H20	122.6	C18–C16–H20	119.7	C15–C18–C16	123.5
C15–C18–N21	118.0	C16–C18–N21	118.5	C18–N21–O22	117.7
C18–N21–O23	117.3	O22–N21–O23	125.1		

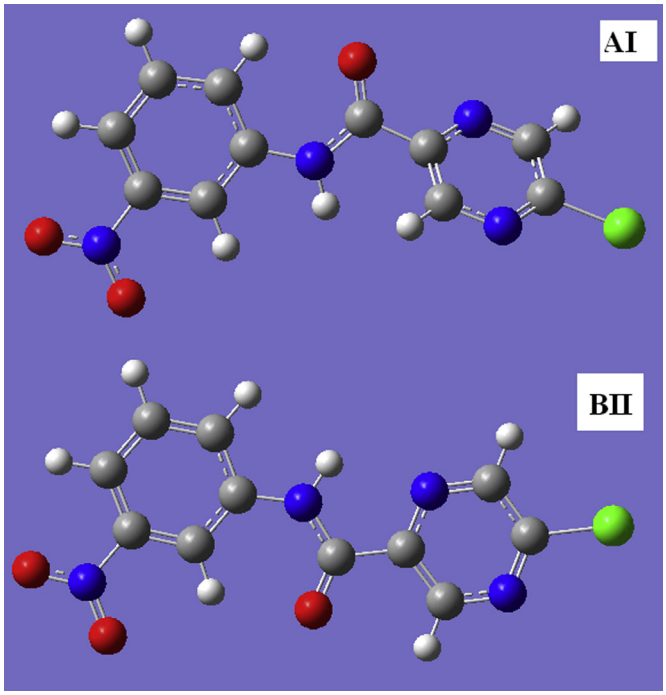

Fig. 4. Possible conformations of 5-chloro-*N*-(3-nitrophenyl)pyrazine-2-carboxamide with respect to the dihedral angle C10–O25–N11–H24.

48.25 with PEDs, 51, 62, 40%. The reported values of NO_2 modes are 1593, 1431 (stretching), 744 (IR), 772, 736 (IR), 779, 737 cm^{-1} (DFT) [34] and at 1621, 1582, 1526, 1328 (IR), 1601, 1585, 1561, 1532, 1347, 1343, 1332 cm^{-1} (DFT) [37] and at 744 (IR), 821, 716 cm^{-1} (DFT) [38].

4.2.2. C = O modes

For the title compound, the C=O stretching and deformation modes are assigned at 1694 (IR), 1696 (Raman), 1699 cm^{-1} (DFT) and 764 (IR), 666 (Raman), 664, 760 cm^{-1} (DFT) which are in agreement with reported literature [34,39,40]. The C=O stretching mode has an IR intensity of 194.89 and Raman activity of 181.54 with a PED of 80%. Raju et al. [41] reported the C=O modes at 1654, 795, 580 (IR), 1659, 798, 577 cm^{-1} (DFT), for a similar derivative.

4.2.3. NH and CN modes

The N–H stretching mode is expected in the region 3500–3300 cm^{-1} and the N–H deformations at around 1500 cm^{-1} and 1250 cm^{-1} [39,42] and for the title compound, these modes are assigned at 3462, 3324 (IR), 3450 cm^{-1} (Raman), 3400 cm^{-1} (DFT) (stretching), 1508, 1219 cm^{-1} (DFT). For the title compound, the theoretical calculation gives a PED of 99% for the NH stretching mode with IR intensity of 97.13 and Raman activity of 226.17. The NH stretching mode is a doublet in the IR spectrum with a difference of 138 cm^{-1} and is red shifted by 76 cm^{-1} from the computed value, which indicates the weakening of NH bond resulting in proton transfer to the neighboring oxygen atom. The reported values of N–H modes are at 1587, 1250, 650 (IR), 1580, 1227, 652 cm^{-1} (DFT) [43]. In the present case, the N–H out-of-plane mode is assigned 655 cm^{-1} theoretically [36] and the reported values for a similar derivative are 762 (IR), 757 cm^{-1} (DFT) [41]. The C–N stretching modes are expected in the region 1100–1300 cm^{-1} [44] and in the present case the bands at 1110, 924 cm^{-1} in IR, 1110, 918 cm^{-1} in Raman, 1219, 1111, 921 cm^{-1} theoretically are assigned as these modes which are in agreement with literature [41].

Aromatic nitro compounds show a C–N stretching vibration near [44] 870 cm^{-1} and the band at 897 cm^{-1} theoretically is assigned as the C–N stretching mode of nitro group attached with the phenyl ring for the title compound. Out of the four C–N stretching modes, corresponding to the mode 1219 (DFT), the IR intensity is 39.14 and Raman activity is 342.14 with a PED of 47% and experimentally no bands are observed and for the mode at 897 (DFT), the IR intensity and Raman activity are low and the corresponding bands are absent experimentally as expected. But for the modes at 1111, 921 (DFT), the IR intensities and Raman activities are moderate and bands are observed experimentally in both the spectra with PEDs 48 and 40%. The C–N stretching modes are reported at 1258, 1245, 1103, 897 cm^{-1} (DFT) [34], 1215 cm^{-1} (DFT) [45].

Table 2
Calculated (scaled) wavenumbers, observed IR, Raman bands and assignments of 5-chloro-*N*-(3-nitrophenyl)pyrazine-2-carboxamide.

B3LYP/CC-pVDZ (5D, 7F)			IR	Raman	Assignments[a]
υ(cm^{-1})	IR_I	R_A	υ(cm^{-1})	υ(cm^{-1})	–
3400	97.13	226.17	3462, 3324	3450	υNH(99)
3147	22.91	25.17	–	–	υCHPh(99)
3121	4.69	120.94	3120	3118	υCHPh(97)
3088	0.79	80.38	3090	–	υCHPz(99)
3078	8.82	165.25	–	–	υCHPh(97)
3071	6.09	99.36	3071	–	υCHPz(99)
3052	7.83	59.30	3052	3055	υCHPh(99)
1699	194.89	181.54	1694	1696	υC = O(80)
1615	2.72	144.39	1618	1620	υPh(52), υNO_2(29)
1578	37.97	84.72	–	1585	υPh(49), υNO_2(18)
1568	361.12	178.80	1566	1565	υNO_2(54), υPh(27)
1545	32.79	593.16	1540	1540	υPz(64), δCHPz(15)
1517	7.53	51.12	–	–	υPz(77)
1508	604.75	745.17	–	–	δNH(46), υCN(20)
1452	19.98	16.82	1452	1457	δCHPh(20), υPh(57)
1421	41.23	118.81	1424	1425	δCHPz(21), υPz(53)
1409	113.37	66.86	–	1410	υPh(44), δCHPh(21)
1342	270.96	120.14	1345	1345	υNO_2(83), υCN(15)
1327	90.39	152.37	1330	–	υPh(80)
1305	68.15	62.07	–	1302	υPz(59), υPh(22)
1255	29.34	60.40	–	–	δCHPz(49), υPz(26)
1240	9.91	4.37	1242	1242	δCHPz(45), δCHPh(39)
1225	12.88	40.58	–	–	υPz(55), δCHPh(10)
1219	39.14	342.14	–	–	υCN(47),δNH(40)
1200	38.71	137.32	–	1198	υPz(57), δCHPz(11)
1135	2.70	6.75	1136	1140	δCHPh(78)
1111	163.70	18.17	1110	1110	υCN(48), δCHPz(15)
1092	83.15	51.34	1088	–	υPz(46), υCN(11)
1064	3.47	9.61	–	1068	υPh(15), δCHPh(58)
1050	54.94	0.50	–	1048	δCHPh(44), υPh(28)
996	54.86	4.43	997	998	δPz(52), υPz(24)
973	0.31	80.12	–	974	δPh(22), υPh(49)
960	0.25	0.69	–	–	γCHPh(86), τPh(10)
946	1.89	1.87	944	945	γCHPz(80), τPz(10)
930	10.82	1.54	–	–	γCHPh(72)
921	8.39	5.31	924	918	υCN(40), υPh(12)
897	5.34	0.47	–	–	γCHPz(50), υCN(39)
889	0.88	1.99	889	886	γCHPh(80)
869	44.87	3.58	–	864	δC = O(21), δCN(15), δPz(17)
808	26.99	5.04	811	810	δNO_2(51), δPh(10)
788	11.87	1.21	789	–	γCHPh(55), τPh(18), γNO_2(17)
779	3.87	2.81	–	776	τPz(52), γCC(18), γC = O(13)
760	11.35	19.30	764	–	δPz(16), υCCl(44), δC = O(32)
726	29.49	2.52	724	730	γNO_2(62), γCHPh(16)
698	3.86	0.80	–	700	τPz(37), γC = O(36), γCCl(11)
673	48.00	1.23	675	–	τPh(57), γCN(10)
664	13.95	7.22	–	666	δPh(25), δNO_2(22), δC = O(35)
655	18.19	1.16	–	–	τPh(15), γNH(43), γCN(11)
618	1.65	12.59	–	615	δPz(67), γNH(10), γCN(11)
576	4.98	8.49	580	577	δPh(56), τPh(14), γNO_2(10)
539	2.49	0.31	541	–	γCN(29), τPh(39), γNO_2(19)
528	14.25	5.32	526	530	δNO_2(40), δC = O(19)
505	8.71	2.60	–	–	δNO_2(39), υCCl(17), δC = O(10)
487	4.13	0.08	485	485	γCCl(33), τPz(31), γCC(19)
428	0.19	0.30	430	–	τPh(66), γNO_2(17)
419	21.88	5.68	–	421	δCCl(31), δCC(14), δPh(10)
408	11.38	0.14	410	406	τPz(85)
381	4.91	2.41	–	378	δPh(24), δCN(34)
347	1.95	3.31	–	–	δCN(42), δC = O(16), δNO_2(28)
308	4.66	1.44	–	–	δCCl(37), δPz(23), δCC(10)
295	0.30	0.49	–	294	γCC(23), τPh(23), γCCl(12), τC = O(15), γNH(10)
247	7.97	1.36	–	250	δCCl(22), δCN(19), δNO_2(36)
234	0.74	4.23	–	–	τPh(46), γCC(13)
221	0.44	0.53	–	221	δCCl(13), δPz(16), δCC(22), δPh(22)
167	0.82	2.41	–	–	τPh(27), τNO_2(60)
123	1.56	0.59	–	130	δCN(42), δCC(17), δC = O(14)
95	0.84	2.07	–	95	τCC(47), τNH(38)
88	2.37	0.93	–	–	τPz(50), τCC(25), τC = O(13)
54	0.85	0.43	–	–	δCN(39), δC = O(26), δCC(18)
52	0.05	0.80	–	–	τNO_2(58), τCC(15)
37	0.16	1.22	–	–	τNH(50), τNO_2(19), τCC(11)
23	0.06	0.30	–	–	τC = O(31), τNH(33)

[a] υ-stretching; δ-in-plane deformation; γ-out-of-plane deformation; τ-torsion; Ph-phenyl ring; Pz-pyrazine ring; IR_I-IR intensity; R_A-Raman activity; potential energy distribution (%) is given in brackets in the assignment column.

4.2.4. C–Cl modes

The C–Cl stretching vibrations give bands in the region 710–505 cm^{-1} and for simple organic chlorine compounds the C–Cl absorptions are in the region 750–700 cm^{-1} [36]. Renjith et al. [46,47] reported the C–Cl stretching modes in the region 609–947 cm^{-1} and Resmi et al. [48] reported C–Cl stretching modes at 876, 644, 581 cm^{-1} in Raman spectrum and at 877, 646, 588 cm^{-1} theoretically. In the present case the C–Cl stretching mode is assigned at 764 cm^{-1} in the IR spectrum and at 760 cm^{-1} theoretically with IR intensity 11.35, Raman activity 19.30 and a PED of 44%.

4.2.5. Pyrazine ring modes

The pyrazine C–H stretching modes are observed at 3090, 3071 cm^{-1} in the IR spectrum and at 3088, 3071 cm^{-1} theoretically with PED 99% which are expected in the range 3000–3100 cm^{-1} [49]. The pyrazine ring stretching modes are assigned at 1540, 1424 (IR), 1540, 1425, 1302, 1198 (Raman) and in the range 1545–1200 cm^{-1} theoretically. Almost for all the modes the IR intensity and Raman activities are high and the PED values are from 53% to 64%. Lukose et al. [27] reported pyrazine ring stretching modes at 1545, 1153, 1059, 985 cm^{-1} experimentally and at 1550, 1518, 1193, 1152, 1045, 982 cm^{-1} theoretically. The ring breathing mode of the 1,4- substituted pyrazine ring is reported at 1120 (IR), 1124 (Raman), 1126 cm^{-1} theoretically [50] and 1131 cm^{-1} [51] and for the title compound the ring breathing mode of the pyrazine ring is assigned at 1092 cm^{-1} (DFT) and 1088 cm^{-1} (IR). The ring breathing mode has a IR intensity of 83.15 and PED value of 46%. The CH deformation modes of the pyrazine ring are assigned at 1242 (IR), 1242 (Raman), 1255, 1240 cm^{-1} (DFT) with PEDs 49 and 45% (in-plane bending) and 944 (IR), 945 (Raman), 946, 897 cm^{-1} (DFT) (out-of-plane bending) with PEDs 80 and 50% as expected [36,40].

4.2.6. Phenyl ring modes

For the title compound, the phenyl C–H stretching modes are assigned at 3120, 3052 (IR), 3118, 3055 (Raman) and 3147, 3121, 3078, 3052 cm^{-1} (DFT) as expected [36]. The PEDs of these modes are almost 100%. The phenyl ring stretching modes are expected in the range 1615–1260 cm^{-1} [36] and for the title compound, the bands observed 1618, 1452, 1330 (IR), 1620, 1585, 1457, 1410 (Raman) and in the range 1615–1327 cm^{-1} theoretically. All the phenyl ring stretching modes are IR and Raman active according to the theoretical calculations and having PEDs in the range 44–80%. The sixth phenyl ring stretching mode or ring breathing mode appears as a weak band near 1000 cm^{-1} in 1,3-di substituted benzene and in the present case this mode is assigned at 973 cm^{-1} theoretically as expected [36,52]. For the title compound, the ring breathing mode has low IR intensity (0.31) and Raman activity (8.12) according to the calculations and no band is observed experimentally. The ring breathing mode is reported at 983 cm^{-1} theoretically by Raju et al. [41]. For the title compound, the in-plane and out-of-plane C–H modes of the phenyl ring are assigned at 1242, 1136 (IR), 1242, 1140, 1068, 1048 (Raman), 1240, 1135, 1064, 1050 cm^{-1} (DFT) (in-plane deformation) and 889, 789 (IR), 886 (Raman), 960, 930, 889, 788 cm^{-1} (DFT) (out-of-plane deformation) as expected [36]. The in-plane CH bending modes have PED values of 39, 78, 58 and 44% and out-of-plane bending modes have these values of 86, 72, 80 and 55%.

The RMS error of the observed IR and Raman modes are 3.55 and 3.28 respectively for B3LYP/CC-pVDZ (5D, 7F) methods. The small difference is due to the fact that experimental results belong to the solid phase and theoretical calculations belong to gaseous phase.

4.3. NMR spectra

The absolute isotropic chemical shielding was calculated by B3LYP/GIAO model [53] and relative chemical shifts were then estimated by using the corresponding TMS shielding: σ_{calc}(TMS) calculated previously at the same theoretical level. Numerical values of chemical shift $\delta_{calc} = \sigma_{calc}$(TMS) - σ_{calc} together with calculated values σ_{calc}(TMS), are given in Tables 3 and 4. The experimental values are: ^{1}H NMR (500 MHz, DMSO) δ: 11.27 (bs, 1H, NH), 9.14 (d, J = 1.5 Hz, 1H), 8.96 (d, J = 1.3 Hz, 1H), 8.92 (t, J = 2.2 Hz, 1H), 8.31–8.26 (m, 1H), 8.01–7.97 (m, 1H), 7.67 (t, J = 8.2 Hz, 1H). ^{13}C NMR (125 MHz, DMSO):δ: 161.78, 151.41, 148.1, 144.4, 143.5, 143.2, 139.5, 130.3, 126.9, 119.0 and 115.1.

Looking at the predicted and measured δ values for ^{13}C NMR spectrum, the biggest difference can be observed for the carboxamide carbon (C10), followed by the chloro substituted pyrazine ring carbon (C1). According to predicted values, C1 should have higher δ than C10 of carboxamide. In real world, it is the opposite way. From the measured spectrum, we have assigned the carboxamide C10 to the peak of 161.78 ppm and chloro substituted C1 to 151.41 ppm. This assignment is based on the shifts of similar relevant derivatives. For example the reported δ values for the carboxamide carbon (measured in DMSO-d_6 at ambient temperature) are: *N*-phenylpyrazine-2-carboxamide −160.5 ppm ($CDCl_3$) [54], pyrazine-2-carboxamide − 165.0 ppm(DMSO-d_6) [55].The typical δ for chloro substituted carbon of pyrazine nucleus can be taken from 2-chloropyrazine −148.6 ppm (DMSO-d_6) [56]. The ^{1}H and ^{13}C NMR signals were assigned to atoms based on expected shielding and H–H coupling, together with comparison with published data of relevant similar compounds.

4.4. Nonlinear optical properties

Nonlinear optics deals with the interaction of applied electromagnetic fields in various materials to generate new electromagnetic fields, altered in wavenumber, phase, or other physical properties [57]. Quantum chemical calculations have been shown to be useful in the description of the relationship between the electronic structure of systems and its NLO response [58]. The computational approach allows the determination of molecular NLO properties as an inexpensive way to design molecules by analyzing their potential before synthesis and to determine high order hyperpolarizability tensors of the molecules. The calculated values of the dipole moment and polarizability are 6.8 Debye and 2.61 × 10^{-23}e.s.u. The first order hyperpolarizability of the title compound is calculated and is found to be 5.76 × 10^{-30}e.s.u which is comparable with the reported values of similar derivatives [27,50]. The calculated hyperpolarizability of the title compound is 44.31 times that of the standard NLO material urea

Table 3
Comparison of calculated and predicted shifts of ^{13}C NMR spectrum of 5-chloro-*N*-(3-nitrophenyl)pyrazine-2-carboxamide (sorted by decreasing δ measured values).

Atom	Predicted δ (ppm)	Measured δ (ppm)	Difference δ (ppm)
C10	157.60	161.78	−4.18
C1	163.33	151.41	11.92
C18	151.35	148.04	3.31
C5	147.80	144.40	3.40
C2	143.60	143.46	0.14
C4	143.45	143.18	0.38
C13	140.26	139.48	0.78
C14	129.88	130.24	−0.36
C12	123.19	126.87	−3.68
C16	121.28	118.98	2.30
C15	116.87	115.05	1.83

Table 4
Comparison of calculated and predicted shifts of ^{1}H NMR spectrum of 5-chloro-*N*-(3-nitrophenyl)pyrazine-2-carboxamide (sorted by decreasing δ measured values).

Atom	Predicted δ (ppm)	Measured δ (ppm)
H24	9.3363	11.27
H8	9.8788	9.14
H7	8.867	8.96
H19	10.3734	8.92[a]
H26	7.3884	8.29[a]
H20	8.5686	7.99
H17	7.9448	7.67

[a] Middle of a multiplet.

(0.13×10^{-30}e.s.u) [59] The theoretical second order hyperpolarizability was calculated using the Gaussian09 software and is equal to -20.23×10^{-37} e.s.u. We conclude that the title compound and its derivatives are an attractive object for future studies of nonlinear optical properties. For the title compound, the calculated C–N distances in the molecular structure are intermediate between those of C–N single and C=N double bond and therefore, the calculated data suggest an extended π-electron delocalization of the pyrazine ring and carboxamide moiety [60] which is responsible for the nonlinearity of the molecule.

4.5. Frontier molecular orbitals

The Highest Occupied Molecular Orbital (HOMO) and the Lowest Unoccupied Molecular Orbital (LUMO) are the main orbital take part in chemical stability. The HOMO represents the ability to donate an electron, LUMO as an electron acceptor represent the ability to obtain an electron. The HOMO-LUMO energy gap shows that the energy gap reflects the chemical reactivity and the level of conductivity of the molecule [61]. Smaller the value of energy gap, the easier electron transfer occurs from HOMO to LUMO. Relatively large gap means the molecule would not be kinetically stable [62]. In the present case the energy values of HOMO and LUMO are −8.059 and −4.974 eV, respectively. The ionization energy and electron affinity can be expressed as: I = -E_{HOMO} and A = -E_{LUMO}: I = 8.059 eV and A = 4.974 eV. The different global descriptors are given by, hardness η = (I-A)/2, chemical potential μ = −(I + A)/2 and electrophilicity index ω = $\mu^2/2\eta$ [63,64]. In the present case the values of these descriptors are η = 1.543, μ = −6.516 and ω = 13.00 and the energy gap between HOMO and LUMO orbitals is 3.085 eV Fig. 5 shows the distributions of the HOMO and LUMO orbitals and the HOMO is localized over the entire molecule except NO_2 and the nitrogen atom of the pyrazine ring (away from the chlorine atom) and the LUMO is over the entire molecule, except the NH group. Both the HOMO and LUMO are mainly localized on the pyrazine ring, indicating that the HOMO-LUMO are mostly the π-antibonding type orbital.

4.6. Molecular electrostatic potential and Fukui functions

Molecular electrostatic potential (MEP) is related to the electronic density which is a very useful descriptor in understanding sites for nucleophilic reactions or electrophilic attack [65–67]. To visually consider the most probable sites of the title compound for an interaction with nucleophilic and electrophilic species, MEP was calculated at B3LYP/CC-pVDZ (5D, 7F) level of optimized geometry. The electrophilic reactivities are visualized by red colour which indicates the negative regions of the molecule and the nucleophilic reactivity regions are coloured by blue, indicating positive regions of the molecule (Fig. 6). In the present case, the electrophilic regions are oxygen atoms and nucleophilic regions are mainly NH group and nitrogen atoms (Fig. 6).

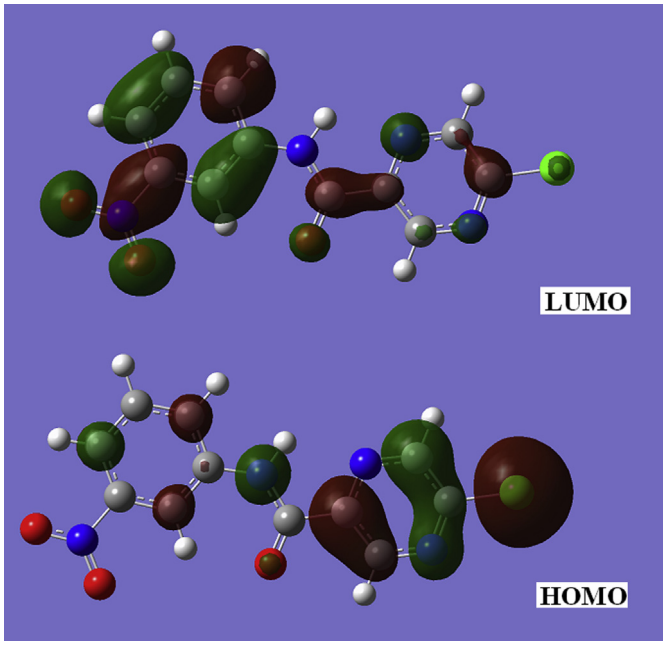

Fig. 5. HOMO-LUMO plots of 5-chloro-*N*-(3-nitrophenyl)pyrazine-2-carboxamide.

The Fukui function is a local reactivity descriptor which gives the preferred regions where a chemical species will change its density when the number of electrons is modified. Hence, Fukui function indicates the propensity of the electronic density to deform at a given position upon accepting or donating electrons [68–70] and the corresponding condensed or atomic Fukui functions on the jth atom site are given as,

$$f_j^- = q_j(N) - q_j(N-1)$$

$$f_j^+ = q_j(N+1) - q_j(N)$$

$$f_j^0 = \frac{1}{2}\left[q_j(N+1) - q_j(N-1)\right]$$

In the above equations, q_j is the atomic charge (evaluated from Mulliken population analysis, electrostatic derived charge, etc.) at jth atomic site is the neutral (N), anionic (N + 1) or cationic (N −1) chemical species. Chattarajet al. [71] have introduced the concept of generalized philicity and it contains almost all information about the known different global and local reactivity and selectivity

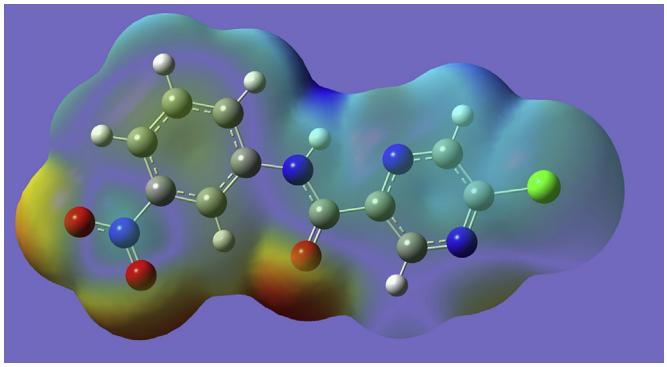

Fig. 6. MEP plot of 5-chloro-*N*-(3-nitrophenyl)pyrazine-2-carboxamide.

descriptor, in addition to the information regarding electrophilic/nucleophilic power of a given atomic site in the molecule. Toro-Labbe et al. [72] proposed a dual descriptor (Δf(r)), which is defined as the difference between the nucleophilic and electrophilic Fukui function and is given by,

$$\Delta f(r) = \left[f^{+}(r) - f^{-}(r)\right]$$

$\Delta f(r) > 0$, then the site is favoured for a nucleophilic attack, whereas if $\Delta f(r) < 0$, then the site may be favoured for an electrophilic attack.

Under this situation, the reactivity descriptors, Δf(r) provides useful information on both stabilising and destabilising interactions between a nucleophile and an electrophile and helps in identifying the electrophilic/nucleophilic behaviour of a specific site within a molecule. It provides positive value for nucleophilic attack and a negative value for electrophilic attack and the results are tabulated in Table 5. The behaviour of molecules as electrophiles/nucleophiles during reaction depends on the local behaviour of molecules.

4.7. Natural bond orbital analysis

The natural bond orbital (NBO) calculations were performed using NBO 3.1 program [73] as implemented in the Gaussian09 package at the DFT/B3LYP level and the possible intensive interactions [74,75] are given in Table 6.

The strong intra-molecular hyper-conjugative interactions are: C_4–C_5 from N_3 of $n_1(N_3)\rightarrow\sigma^*(C_4–C_5)$, C_1–C_2 from N_6 of $n_1(N_6)\rightarrow\sigma^*(C_1–C_2)$, C_1–N_6 from Cl_9 of $n_3(Cl_9)\rightarrow\pi^*(C_1–N_6)$, C_{10}–O_{25} from N_{11} of $n_1(N_{11})\rightarrow\pi^*(C_{10}–O_{25})$, N_{21}–O_{23} from O_{22} of $n_2(O_{22})\rightarrow\pi^*(N_{21}–O_{23})$, N_{21}–O_{22} from O_{23} of $n_3(O_{23})\rightarrow\pi^*(N_{21}–O_{22})$, C_{10}–N_{11} from O_{25} of $n_2(O_{25})\rightarrow\sigma^*(C_{10}–N_{11})$ and the corresponding electron densities and stabilization energies are: 0.03614, 0.04400, 0.39466e, 0.32335, 0.05769, 0.62811, 0.06933e and 8.90, 10.08, 13.46, 67.12, 17.85, 150.88, 23.44 kJ/mol.

The bonding in terms of the natural hybrid orbitals with considerable p characters are: $n_3(Cl_9)$, $n_2(O_{22})$, $n_3(O_{23})$, $n_2(O_{25})$ with a higher energy orbitals −0.33898, −0.28828, −0.27097, −0.26859 a.u and low occupation numbers 1.92043, 1.90368, 1.44780, 1.87210. The bonding orbitals with low p characters are: $n_1(Cl_9)$, $n_1(O_{22})$, $n_1(O_{23})$, $n_1(O_{25})$ with lower energy orbitals −0.93826, −0.80903, −0.81052, −0.71211 a.u and high occupation numbers 1.99474, 1.80903, 1.98270, 1.97656.

Thus, a very close to pure p-type lone pair orbital participates in the electron donation to the $\sigma^*(C_4–C_5)$ orbital for $n_1(N_3)\rightarrow\sigma^*(C_4–C_5)$, $\sigma^*(C_1–C_2)$ orbital for $n_1(N_6)\rightarrow\sigma^*(C_1–C_2)$, $\pi^*(C_1–N_6)$ orbital for $n_3(Cl_9)\rightarrow\pi^*(C_1–N_6)$, $\pi^*(C_{10}–O_{25})$ orbital for $n_1(N_{11})\rightarrow\pi^*(C_{10}–O_{25})$, $\sigma^*(N_{21}–O_{23})$ orbital for $n_2(O_{22})\rightarrow\sigma^*(N_{21}–O_{23})$, $\sigma^*(N_{21}–O_{22})$ orbital for $n_3(O_{23})\rightarrow\sigma^*(N_{21}–O_{22})$, and $\sigma^*(C_{10}–N_{11})$ orbital for $n_2(O_{25})\rightarrow\sigma^*(C_{10}–N_{11})$ interaction in the compound. The results are tabulated in Table 7.

Table 5
Values of the Fukui function considering Mulliken charges.

Atom	f_j^-	f_j^+	Δf_k
C1	−0.074540	0.130076	0.204618
C2	0.145306	−0.100550	−0.245860
N3	0.150167	−0.294150	−0.444320
C4	0.051460	0.227258	0.175798
C5	0.127521	−0.102580	−0.230100
N6	0.216175	−0.229950	−0.446130
H7	−0.024170	0.209248	0.233419
H8	−0.022890	0.200820	0.223714
Cl9	0.212819	0.172673	−0.040150
C10	−0.055380	0.433824	0.489206
N11	0.252383	−0.564460	−0.816850
C12	0.106391	−0.166890	−0.273290
C13	−0.058940	0.314788	0.373729
C14	0.120622	−0.197780	−0.318400
C15	0.138753	−0.192910	−0.331660
C16	0.135301	−0.139100	−0.274400
H17	−0.073060	0.244906	0.317961
C18	0.024782	0.168245	0.143463
H19	−0.100480	0.257879	0.358357
H20	−0.077150	0.260078	0.337230
N21	0.007088	0.233355	0.226267
O22	−0.027570	−0.117540	−0.089970
O23	−0.017230	−0.104300	−0.087070
H24	−0.142830	0.320085	0.462915
O25	0.068535	−0.202010	−0.270550
H26	−0.083060	0.238988	0.322046

4.8. Molecular docking

Pyrazine-2-carboxamide derivatives showed antimicrobial activity [76] and Cathepsin K is a lysosomal cysteine protease that has pleiotropic roles in bone resorption, arthritis, atherosclerosis, blood pressure regulation obesity and cancer. The extracellular cathepsin K is an intestinal antibacterial factor with anti-inflammatory potential and suggests that topical administration of cathepsin K might provide a therapeutic option for patients with inflammatory bowel disease [77]. Thus we selected the target macromolecule for docking simulation. High resolution 3D crystal structure of cathepsin K was downloaded from the Protein Data Bank website (PDB ID: 1SNK). All molecular docking calculations were performed on Auto Dock-Vina software [78]. The protein was prepared for docking by removing the co-crystallized ligands, waters and co-factors. The Auto Dock Tools (ADT) graphical user interface was used to calculate Kollman charges and polar hydrogens. The ligand was prepared for docking by minimizing its energy at B3LYP/CC-pVDZ (5D, 7F) level of theory. Partial charges were calculated by Geistenger method. The active site of the enzyme was defined to include residues of the active site within the grid size of 40 Å × 40 Å × 40 Å. The docking protocol was tested by extracting co-crystallized inhibitor from the protein and then redocking the same. The docking protocol predicted the same conformation as was present in the crystal structure with RMSD value well within the reliable range of 2 Å [79]. Amongst the docked conformations of the title ligand, one which binds well at the active site was analyzed for detailed interactions in Discover Studio Visualizer 4.0 software. The ligand binds at the active site of the substrate (Figs. 7 and 8) by weak non-covalent interactions. Amino acids Asn161, His162 forms H-bond with pyrazine ring and Trp184, Gln19 shows H-bond with C═O group. The docked ligand title compound forms a stable complex with cathepsin K and gives a binding affinity (ΔG in kcal/mol) value of −6.7 (Table 8). These preliminary results suggest that the compound might exhibit inhibitory activity against cathepsin K.

4.9. In vitro antiviral activity

As a complementary test, the title compound was tested for potential activity against diverse DNA and RNA viruses of medical importance (Section 2.3). Table 9 summarized detected antiviral activities. Moderate activity with EC_{50} at tens of μM was detected for feline herpes virus and coxsackie virus B4. Activity against coxsackie B4 virus was detected in CRFK cells, but not in HeLa cells. Similar activity was detected against two strains of influenza A, both H1N1 (A/Virginia/ATCC3/2009) and H3N2 (A/HK/7/87). According to EC_{50} values determined by MTS assay, the antiviral activity of the title compound was comparable to standard zanamivir or ribavirin. Influenza A/H1N1 (A/PR/8) was resistant. Influenza B virus (B/HK/5/72) was resistant. Other tested strains not explicitly

Table 6
Second order perturbation theory analysis of Fock matrix in NBO basis corresponding to the intra-molecular bonds of the title compound.

Donor(i)	Type	ED/e	Acceptor(j)	Type	ED/e	E(2)[a]	E(j)-E(i)[b]	F(i,j)[c]
C1–C2	σ	1.99175	C1–N6	σ*	0.02802	1.58	1.28	0.040
C1–N6	σ	1.98900	C1–C2	σ*	0.04400	1.87	1.40	0.046
_	π	1.71624	C2–N3	π*	0.33801	17.55	0.31	0.067
_	–	–	C4–C5	π*	0.29095	21.28	0.34	0.076
C1–Cl9	σ	1.98678	C2–N3	σ*	0.01617	2.84	1.18	0.052
_	–	–	C5–N6	σ*	0.01365	3.29	1.17	0.055
C4–C5	σ	1.98687	N3–C4	σ*	0.02350	1.49	1.23	0.038
_	–	–	C4–C10	σ*	0.07087	2.09	1.15	0.045
_	–	–	C10–N11	σ*	0.06933	1.77	1.21	0.042
C4–C10	σ	1.97533	C2–N3	σ*	0.01617	3.07	1.18	0.054
_	–	–	N3–C4	σ*	0.02350	1.07	1.16	0.032
_	–	–	C4–C5	σ*	0.03614	1.45	1.22	0.038
_	–	–	C5–N6	σ*	0.01365	2.50	1.17	0.048
_	–	–	N11–C13	σ*	0.02810	4.14	1.10	0.060
C10–N11	σ	1.98925	C4–C5	σ*	0.03614	1.54	1.37	0.041
_	–	–	N11–C13	σ*	0.02810	1.96	1.26	0.045
_	–	–	C12–C13	σ*	0.02002	1.60	1.38	0.042
C10–O25	π	1.97278	C4–C5	π*	0.29095	4.13	0.36	0.037
C13–C15	π	1.61698	C12–C14	π*	0.32116	19.50	0.28	0.067
_	–	–	C16–C18	π*	0.38571	21.08	0.28	0.069
C18–N21	σ	1.99013	C13–C15	σ*	0.35624	1.66	1.36	0.042
_	–	–	C14–C16	σ*	0.01506	1.46	1.38	0.040
N21–O22	π	1.98470	C16–C18	π*	0.38571	4.61	0.44	0.045
_	–	–	N21–O22	π*	0.62811	7.11	0.30	0.049
LPN3	σ	1.91230	C1–C2	σ*	0.04400	8.81	0.89	0.080
_	–	–	C4–C5	σ*	0.03614	8.90	0.92	0.082
_	–	–	C4–C10	σ*	0.07087	2.31	0.79	0.038
LPN6	σ	1.90124	C1–C2	σ*	0.04400	10.08	0.88	0.085
_	–	–	C1–Cl9	σ*	0.07263	5.20	0.46	0.044
_	–	–	C4–C5	σ*	0.03614	8.76	0.90	0.081
LPCl9	σ	1.99474	C1–C2	σ*	0.04400	1.13	1.43	0.036
_	π	1.97023	C1–C2	σ*	0.04400	3.10	0.83	0.045
_	–	–	C1–N6	σ*	0.02802	5.09	0.83	0.058
_	n	1.92043	C1–N6	π*	0.39466	13.46	0.29	0.060
LPN11	σ	1.63626	C10–O25	π*	0.32335	67.12	0.26	0.120
_	–	–	C13–C15	π*	0.35624	34.88	0.29	0.090
LPO22	σ	1.98254	C18–N21	σ*	0.09412	4.21	1.09	0.062
_	–	–	N21–O23	σ*	0.05769	1.98	1.16	0.043
_	π	1.90368	C18–N21	σ*	0.09412	10.40	0.57	0.069
_	–	–	N21–O23	σ*	0.05769	17.85	0.64	0.096
LPO23	σ	1.98270	C18–N21	σ*	0.09412	4.14	1.09	0.061
_	–	–	N21–O22	σ*	0.05657	1.98	1.17	0.043
_	π	1.90569	C18–N21	σ*	0.09412	10.16	0.57	0.068
_	–	–	N21–O22	σ*	0.05657	17.48	0.65	0.096
_	n	1.44780	N21–O22	π*	0.62811	150.88	0.13	0.128
LPO25	σ	1.97656	C4–C10	σ*	0.07087	2.12	1.10	0.044
_	–	–	C10–N11	σ*	0.06933	2.27	1.16	0.046
_	π	1.87210	C4–C10	σ*	0.07087	18.61	0.66	0.100
_	–	–	C10–N11	σ*	0.06933	23.44	0.71	0.117

[a] E(2) means energy of hyper-conjugative interactions (stabilization energy in kJ/mol).
[b] Energy difference (a.u.) between donor and acceptor i and j NBO orbitals.
[c] F(i,j) is the Fock matrix elements (a.u.) between i and j NBO orbitals.

mentioned in Table 9 were completely resistant. The basis for the antiviral effect of 5-chloro-*N*-(3-nitrophenyl)pyrazine-2-carboxamide remains to be identified.

4.10. *In vitro* cytotoxicity

In vitro cytotoxicity of 5-chloro-*N*-(3-nitrophenyl)pyrazine-2-carboxamide on different animal and human cell lines was evaluated during the testing of antiviral activity as a control (see Section 2.3 for the list of used cell lines). The toxicity was measured as either CC_{50} (concentration reducing the cell viability by 50% as measured by formazan-based colorimetric assay) or as MCC (minimum compounds concentration to cause microscopically detectable alteration of normal cell morphology). With the exception of human MT-4 lymphoblasts (CC_{50} = 13 μM) and Madin-Darby canine kidney (MDCK) cells (MCC ≥ 20 μM; although CC_{50} > 100 μM), no cytotoxicity was detected up to the concentration of 100 μM. This rather low or none cytotoxicity of 5-chloro-*N*-(3-nitrophenyl)pyrazine-2-carboxamide is consistent with the previously published study, which evaluated *in vitro* cytotoxicity of

Table 7
NBO results showing the formation of Lewis and non-Lewis orbital.

Bond(A-B)	ED/e[a]	EDA%	EDB%	NBO	s%	p%
σ C1–C2	1.99175	50.71	49.29	0.7121($sp^{1.38}$)C+	41.93	58.07
_	−0.78802	–	–	0.7021($sp^{1.76}$)C	36.22	63.78
σ C1–N6	1.98900	40.87	59.13	0.6393($sp^{1.90}$)C+	34.51	65.49
_	−0.90981	–	–	0.7690($sp^{1.71}$)N	36.76	63.24
π C1–N6	1.71624	44.81	55.19	0.6994($sp^{1.00}$)C+	0.00	100.0
_	−0.35976	–	–	0.7429($sp^{1.00}$)N	0.00	100.0
σ C1–Cl9	1.98678	45.72	54.28	0.6762($sp^{3.25}$)C+	23.49	76.51
_	−0.70066	–	–	0.7368($sp^{5.58}$)Cl	15.14	84.86
σ C4–C5	1.98687	51.38	48.62	0.7168($sp^{1.68}$)C+	37.35	62.65
_	−0.76390	–	–	0.6973($sp^{1.74}$)C	36.54	63.46
σ C4–C10	1.97533	52.16	47.84	0.7222($sp^{2.05}$)C+	32.75	67.25
_	−0.70070	–	–	0.6917($sp^{1.84}$)C	35.16	64.84
σ C10–N11	1.98925	37.16	62.84	0.6096($sp^{2.10}$)C+	32.17	67.83
_	−0.85690	–	–	0.7927($sp^{1.80}$)N	35.75	64.25
π C10–O25	1.97278	30.74	69.26	0.5544($sp^{1.00}$)C+	0.00	100.0
_	−0.37909	–	–	0.8322($sp^{1.00}$)O	0.00	100.0
π C13–C15	1.61698	51.67	48.33	0.7188($sp^{1.00}$)C+	0.00	100.0
_	−0.27731	–	–	0.6952($sp^{1.00}$)C	0.00	100.0
σ C18–N21	1.99013	37.62	62.38	0.6134($sp^{3.13}$)C+	24.19	75.81
_	−0.82072	–	–	0.7898($sp^{1.67}$)N	37.45	62.55
π N21–O22	1.98470	40.36	59.64	0.6353($sp^{1.00}$)N+	0.00	100.0
_	−0.43610	–	–	0.7723($sp^{1.00}$)O	0.00	100.0
n1N3	1.91230	–	–	$sp^{2.49}$	28.63	71.37
_	−0.40443	–	–	–	–	–
n1N6	1.90124	–	–	$sp^{2.50}$	28.48	71.52
_	−0.3868	–	–	–	–	–
n1Cl9	1.99474	–	–	$sp^{0.18}$	85.00	15.00
_	−0.93826	–	–	–	–	–
n2Cl9	1.97023	–	–	$sp^{99.99}$	0.09	99.91
_	−0.33916	–	–	–	–	–
n3Cl9	1.92043	–	–	$sp^{1.00}$	0.00	100.0
_	−0.33898	–	–	–	–	–
n1N11	1.63626	–	–	$sp^{1.00}$	0.00	100.0
_	−0.28525	–	–	–	–	–
n1O22	1.98254	–	–	$sp^{0.29}$	77.33	22.63
_	−0.80903	–	–	–	–	–
n2O22	1.90368	–	–	$sp^{99.99}$	0.24	99.76
_	−0.28828	–	–	–	–	–
n1O23	1.98270	–	–	$sp^{0.29}$	77.50	22.50
_	−0.81052	–	–	–	–	–
n2O23	1.90569	–	–	$sp^{99.99}$	0.23	99.77
_	−0.28894	–	–	–	–	–
n3O23	1.44780	–	–	$sp^{1.00}$	0.00	100.0
_	−0.27093	–	–	–	–	–
n1O25	1.97656	–	–	$sp^{0.62}$	61.80	38.20
_	−0.71211	–	–	–	–	–
n2O25	1.87210	–	–	$sp^{1.00}$	0.00	100.0
_	−0.26859	–	–	–	–	–

[a] ED/e in a.u.

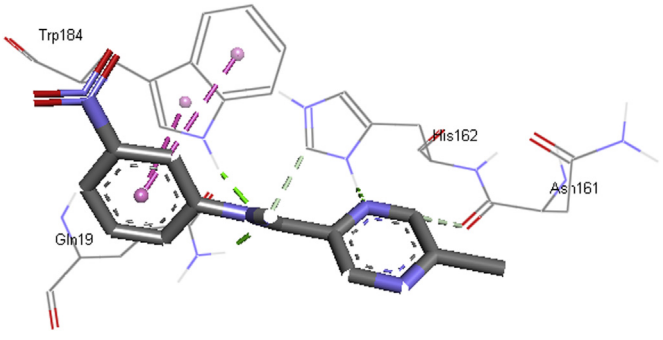

Fig. 7. Schematic for the ligand interaction with the active site of cathepsin K.

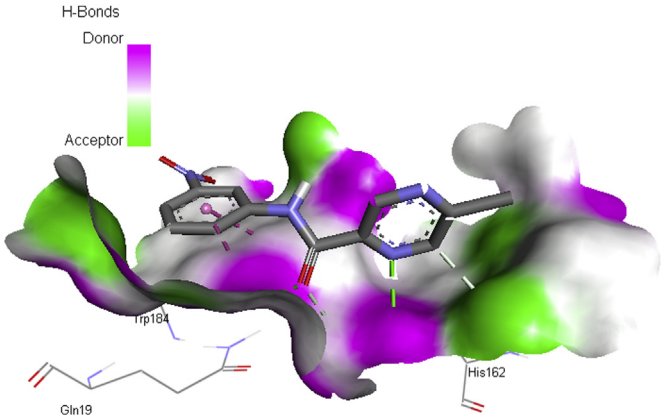

Fig. 8. The docked protocol reproduced the co-crystallized conformation with H-bond (green), π-π (magenta) and H-bond receptor surface shown.

Table 8
The binding affinity values of different poses of the title compound predicted by Autodock Vina.

Mode	Affinity (kcal/mol)	Distance from best mode (Å)	
		RMSD l.b.	RMSD u.b.
1	−6.7	0.000	0.000
2	−6.7	3.808	7.537
3	−6.6	3.764	4.474
4	−6.4	1.614	2.125
5	−6.3	24.331	26.336
6	−6.3	3.906	7.225
7	−6.2	2.844	4.008
8	−6.2	24.481	26.925
9	−6.0	24.166	25.700

5-chloro-*N*-pyrazine-2-carboxamides with various substituents on the phenyl ring on human hepatocellular liver carcinoma cell line HepG2, and the 3-nitrophenyl derivative was one of the least toxic compounds with IC_{50} = 32.7 μM [80].

5. Conclusion

The optimized geometries and vibrational wavenumbers of the title compound have been determined using DFT/B3LYP/CC-pVDZ (5D, 7F) basis set. The vibrational spectra were then assigned and the modes were visualized through the GaussView program. The NH stretching mode is a doublet in the IR spectrum and is red shifted by 76 cm^{-1} from the theoretical wavenumber which indicates the weakening of NH bond. The ring breathing mode of the pyrazine ring is assigned at 1092 cm^{-1} (DFT) and 1088 cm^{-1} (IR) with IR intensity of 83.15 and PED value of 46%. The phenyl ring stretching mode or ring breathing mode is assigned at 973 cm^{-1} theoretically as expected and has low IR intensity (0.31) and Raman activity (8.12) according to the calculations and no band is observed experimentally. The HOMO and LUMO orbitals are mainly localized on the pyrazine ring, indicating that these orbitals mostly the π-anti-bonding type orbital. From the MEP analysis it is evident that the electrophilic regions are oxygen atoms and nucleophilic regions are mainly NH group and nitrogen atoms. Stability of the molecule arising from hyperconjugative interaction and charge delocalization has been analyzed using natural bond orbital analysis. Moderate *in vitro* antiviral activity with EC_{50} at tens of μM was detected against feline herpes virus, coxsackie virus B4, and one strain of influenza A/H1N1 and one strain of influenza A/H3N2. The docked

Table 9
In vitro antiviral activity EC_{50} (μM)[a] and cytotoxicity[b] (μM) of 5-chloro-*N*-(3-nitrophenyl)pyrazine-2-carboxamide in comparison with standards.

Entry	Feline herpes virus infected CRFK[c] cells		Coxsackie virus B4 infected Vero[c] cells		Influenza infected MDCK[c] cells					
	Feline herpes	CRFK toxicity	Coxsackie virus B4	Vero toxicity	Influenza A/H1N1/A/Virginia/ATCC3/2009		Influenza A/H3N2 (A/HK/7/8/7)		MDCK toxicity	
	MTS	CC50	MTS	MCC	CPE	MTS	CPE	MTS	CC50	MTC
1st run	15	>100	34	>100	>100	>100	45	35	>100	100
2nd run	20	>100	45	>100	>100	24	100	9.4	>100	100
3rd run	–	–	–	–	12	21	>100	6.2	>100	≥20
Ganciclovir	0.9	>100	–	–	–	–	–	–	–	–
Ribavirin	–	>250	>250	8.9	8.5	8.5	20	6.6	>100	≥20
Zanamivir	–	–	–	–	19	6.4	6.9	6.8	>100	>100

[a] Antiviral activity was expressed as EC_{50}, defined as the compound concentration which reduces virus-induced cytopathic effect to 50% as determined microscopically (CPE), or by measuring cell viability in the formazan-based MTS assay (MTS).
[b] Cytotoxicity measures: CC_{50} - concentration reducing the cell viability by 50% as measured by formazan-based colorimetric assay; MCC - minimum compounds concentration to cause microscopically detectable alteration of normal cell morphology.
[c] CRFK – Crandell-Rees Feline Kidney cells; MDCK - Madin-Darby canine kidney cells; Vero - African Green Monkey cells.

ligand title compound forms a stable complex with cathepsin K and gives a binding affinity value of −6.7 kcal/mol and this suggests that the compound might exhibit inhibitory activity against cathepsin K.

Acknowledgements

The authors would like to extend their sincere appreciation to the Deanship of Scientific Research at King Saudi University for funding this work through the Research Group Project No. PRG-1436-23. Authors wish to thank Associate Professor Lieve Naesens (Rega Institute for Medical Research, Laboratory of Virology and Chemotherapy, Leuven, Belgium) for coordination of antiviral testing.

References

[1] I.V. Ukrainets, N.L. Bereznyakova, Chem. Heterocycl. Compd. 48 (2012) 155.
[2] M. Dolezal, D. Kesetovic, J. Zitko, Curr. Pharm. Des. 17 (2011) 3506.
[3] P.B. Miniyar, P.R. Murumkar, P.S. Patil, M.A. Barmade, K.G. Bothara, Mini Rev. Med. Chem. 13 (2013) 1607.
[4] R. Mueller, S. Rappert, Appl. Microbiol. Biotechnol. 85 (2010) 1315.
[5] M. Dolezal, J. Zitko, Expert Opin. Ther. Pat. 25 (2015) 33.
[6] C.H.S. Lima, M.L.F. Bispo, M.V.N. de Souza, Rev. Virtual Quim 3 (2011) 159.
[7] K. Konno, F.M. Feldmann, W. McDermott, Am. Rev. Respir. Dis. 95 (1967) 461.
[8] Y. Zhang, M.M. Wade, A. Scorpio, H. Zhang, Z. Sun, J. Antimicrob. Chem. 52 (2003) 790.
[9] S. Martin, C. Revathi, A. Dayalan, N. Mathivannan, V. Shanmugaiya, Rasayan J. Chem. 1 (2008) 378.
[10] J.E. Tomassini, M.E. Davies, J.C. Hastings, R. Lingham, M. Mojena, S.L. Raghoobar, S.B. Singh, J.S. Tkacz, M.A. Goetz, Antimicrob. Agents Chemother. 40 (1996) 1189.
[11] S.B. Singh, J.E. Tomassini, J. Org. Chem. 66 (2001) 5504.
[12] Y. Furuta, K. Takahashi, K. Shiraki, K. Sakamoto, D.F. Smee, D.L. Barnard, B.B. Gowen, J.G. Julander, J.D. Morrey, Antivir. Res. 82 (2009) 95.
[13] S. Zeuzem, P. Anderone, S. Pol, E. Lawitx, M. Diago, S. Roberts, R. Focaccia, Z. Younossi, G.R. Foster, A. Horban, P. Ferenci, F. Nevens, B. Mullhaupt, P. Pockros, R. Terg, D. Shouval, B. van Hoek, O. Weiland, R. Van Heeswijk, S. De Meyer, D. Luo, G. Boogaerts, R. Polo, G. Picchio, M. Beumony, R.S. Team, New Engl. J. Med. 364 (2011) 2417.
[14] B. Servusova, J. Vobickova, P. Paterova, V. Kubicek, J. Kunes, M. Dolezal, J. Zitko, Bioorg. Med. Chem. Lett. 23 (2013) 3589.
[15] L. Naesens, C.E. Stephen, G. Andrei, A. Loregian, L. De Bolle, R. Snoeck, J.W. Sowell, E. De Clercq, Antivir. Res. 72 (2006) 60.
[16] E. Vanderlinden, F. Goktas, Z. Cesur, M. Froeyen, M.L. Reed, C.J. Russell, N. Cesur, L. Naesens, J. Virol. 84 (2010) 4277.
[17] M.J. Frisch, G.W. Trucks, H.B. Schlegel, G.E. Scuseria, M.A. Robb, J.R. Cheeseman, G. Scalmani, V. Barone, B. Mennucci, G.A. Petersson, H. Nakatsuji, M. Caricato, X. Li, H.P. Hratchian, A.F. Izmaylov, J. Bloino, G. Zheng, J.L. Sonnenberg, M. Hada, M. Ehara, K. Toyota, R. Fukuda, J. Hasegawa, M. Ishida, T. Nakajima, Y. Honda, O. Kitao, H. Nakai, T. Vreven, J.A. Montgomery, Jr., J.E. Peralta, F. Ogliaro, M. Bearpark, J.J. Heyd, E. Brothers, K.N. Kudin, V.N. Staroverov, T. Keith, R. Kobayashi, J. Normand, K. Raghavachari, A. Rendell, J.C. Burant, S.S. Iyengar, J. Tomasi, M. Cossi, N. Rega, J.M. Millam, M. Klene, J.E. Knox, J.B. Cross, V. Bakken, C. Adamo, J. Jaramillo, R. Gomperts, R.E. Stratmann, O. Yazyev, A.J. Austin, R. Cammi, C. Pomelli, J W. Ochterski, R.L. Martin, K. Morokuma, V.G. Zakrzewski, G.A. Voth, P. Salvador, J.J. Dannenberg, S. Dapprich, A.D. Daniels, O. Farkas, J.B. Foresman, J.V. Ortiz, J. Cioslowski, D.J. Fox, Gaussian 09, Revision B.01, Gaussian, Inc., Wallingford CT, 2010.
[18] J.B. Foresman, Pittsburg, PA, in: E. Frisch (Ed.), Exploring Chemistry with Electronic Structure Methods: a Guide to Using Gaussian, 1996.
[19] A.D. Becke, J. Chem. Phys. 98 (1993) 5648.
[20] B.K. Paul, N. Guchhait, Comput. Theor. Chem. 1012 (2013) 20.
[21] C. Lee, W. Yang, R.G. Parr, Phys. Rev. B 37 (1988) 785.
[22] E.R. Davidson, Chem. Phys. Lett. 260 (1996) 514.
[23] R. Dennington, T. Keith, J. Millam, Gaussview, Version 5, Semichem Inc., ShawneeMission, KS, 2009.
[24] J.M.L. Martin, C. Van Alsenoy, GAR2PED, a Program to Obtain a Potential Energy Distribution from a Gaussian Archive Record, Universit of Antwerp, Belgium, 2007.
[25] K. Tamagawa, T. Iijima, M. Kimura, J. Mol. Struct. 30 (1976) 243.
[26] K.B. Borisenko, C.W. Bock, I. Hargittai, J. Phys. Chem. 100 (1996) 7426.
[27] J. Lukose, C.Y. Panicker, P.S. Nayak, B. Narayan, B.K. Sarojini, C. Van Alsenoy, A.A. Al-Saadi, Spectrochim. Acta 135 (2015) 608.
[28] V. Chis, A. Piranau, T. Jurca, M. Vasilescu, S. Simon, O. Cozar, L. David, Chem. Phys. 316 (2005) 153.
[29] S.M. Bakalova, A.G. Santos, I. Timcheva, J. Kaneti, I.L. Filipova, G.M. Dobrikov, V.D. Dimitrov, J. Mol. Struct. Theochem 710 (2004) 229.
[30] J.C. Noveron, A.M. Arif, P.J. Stang, Chem. Mater 15 (2003) 372.
[31] H. Takeuchi, M. Sato, T. Tsuji, H. Takashima, T. Egawa, S. Konaka, J. Mol. Struct. 485–486 (1999) 175.
[32] E.D. Stevens, Acta Cryst. 34B (1978) 544.
[33] Q. Gao, G.A. Jeffrey, J.R. Ruble, R.K. McMullan, Acta Cryst. 47B (1991) 742.
[34] C.Y. Panicker, H.T. Varghese, P.S. Nayak, B. Narayana, B.K. Sarojini, H.K. Fun, J.A. War, S.K. Srivastava, C. Van Alsenoy, Spectrochim. Acta 148 (2015) 18.
[35] M. Barthes, G. De Nunzio, M. Ribet, Synth. Met. 76 (1996) 337.
[36] N.P.G. Roeges, A Guide to the Complete Interpretation of Infrared Spectra of Organic Structures, John Wiley and Sons Inc., New York, 1994.
[37] A. Raj, Y.S. Mary, C.Y. Panicker, H.T. Varghese, K. Raju, Spectrochim. Acta 113 (2013) 28.
[38] N. Sundaraganesan, S. Ayyappan, H. Umamaheswari, B.D. Joshua, Spectrochim. Acta 66 (2007) 17.
[39] N.B. Colthup, L.H. Daly, S.E. Wiberly, Introduction of Infrared and Raman Spectroscopy, Academic Press, New York, 1975.
[40] G. Socrates, Infrared Characteristic Group Frequencies, John Wiley and Sons, New York, 1981.
[41] R. Raju, C.Y. Panicker, P.S. Nayak, B. Narayana, B.K. Sarojini, C. Van Alsenoy, A.A. Al-Saadi, Spectrochim. Acta 134 (2015) 63.
[42] L.J. Bellamy, The Infrared Spectrum of Complex Molecules, third ed., Chapman and Hall, London, 1975.
[43] Y.S. Mary, H.T. Varghese, C.Y. Panicker, M. Dolezal, Spectrochim. Acta 71 (2008) 725.
[44] R.M. Silverstein, G.C. Bassler, T.C. Morril, Spectrometric Identification of Organic Compounds, fifth ed., John Wiley and Sons Inc., Singapore, 1991.
[45] C.Y. Panicker, H.T. Varghese, V.S. Madhavan, S. Mathew, J. Vinsova, C. Van Alsenoy, Y.S. Mary, Y.S. Mary, J. Raman Spectrosc. 40 (2009) 2176.
[46] R. Renjith, Y.S. Mary, C.Y. Panicker, H.T. Varghese, M.P. Parys, C. Van Alsenoy, T.K. Manojkumar, Spectrochim. Acta 124 (2014) 500.
[47] R. Renjith, Y.S. Mary, C.Y. Panicker, H.T. Varghese, M.P. Parys, C. Van Alsenoy, T.K. Manojkumar, Spectrochim. Acta 124 (2014) 480.
[48] K.S. Resmi, Y.S. Mary, H.T. Varghese, C.Y. Panicker, M. Pakosinska-Parys, C. Van Alsenoy, J. Mol. Struct. 1098 (2015) 130.
[49] J.F. Arenas, J.T.L. Navarrete, J.I. Marcos, J.C. Otero, J. Chem. Soc. Faraday Trans. 2 (84) (1988) 53.

[50] T. Joseph, H.T. Varghese, C.Y. Panicker, K. Viswathan, M. Dolezal, T.K. Manojukumar, C. Van Alsenoy, Spectrochim. Acta 113 (2013) 203.
[51] H. Endredi, F. Billes, S. Holly, J. Mol. Struct. Theochem 633 (2003) 73.
[52] G. Varsanyi, Assignments of Vibrational Spectra of Seven Hundred Benzene Derivatives, Wiley, New York, 1974.
[53] K. Wolinski, J.F. Hinton, P. Pulay, J. Am. Chem. Soc. 112 (1990) 8251.
[54] Q. Li, S.-Y. Zhang, G. He, Z. Ai, W.A. Nack, G. Chen, Org. Lett. 16 (2014) 1764.
[55] H. Chen, W. Dai, Y. Chen, Q. Xu, J. chen, L. Yu, Y. Zhao, M. Ye, Y. Pan, Green Chem. 16 (2014) 2136.
[56] W. Holzer, G.A. Eller, B. Datterl, D. Habicht, Magn. Reson. Chem. 47 (2009) 617.
[57] Y.R. Shen, The Principles of Nonlinear Optics, Wiley, New York, 1984.
[58] D.M. Burland, R.D. Miller, C.A. Walsh, Chem. Rev. 94 (1994) 31.
[59] M. Adant, M. Dupuis, J.L. Bredas, Int. J. Quantum Chem. 56 (2004) 497.
[60] Y.P. Tian, W.T. Yu, C.Y. Zhao, M.H. Jiang, Z.G. Cari, H.K. Fun, Polyhedron 21 (2002) 1217.
[61] B. Kosar, C. Albayrak, Spectrochim. Acta 78 (2011) 160.
[62] T.E. Rosso, M.W. Elzy, J.O. Jensen, H.F. Hameka, D. Zeroka, Spectrochim. Acta 55 (1998) 121.
[63] R.J. Parr, L.V. Szentpaly, S. Liu, J. Am. Chem. Soc. 121 (1999) 1922.
[64] R.J. Parr, R.G. Pearson, J. Am. Chem. Soc. 105 (1983) 7512.
[65] E. Scrocco, J. Tomasi, Adv. Quantum Chem. 11 (1978) 115.
[66] F.J. Luque, J.M. Lopez, M. Orozco, Theor. Chem. Acc. 103 (2000) 343.
[67] N. Okulik, A.H. Jubert, Internet electron, J. Mol. Des. 4 (2005) 17.
[68] R.G. Parr, W. Yang, Functional Theory of Atoms and Molecules, Oxford University Press, New York, 1989.
[69] P.W. Ayers, R.G. Parr, J. Am. Chem. Soc. 122 (2000) 2010.
[70] R.G. Parr, W.J. Yang, Am. Chem. Soc. 106 (1984) 511.
[71] P.K. Chattaraj, B. Maiti, U. Sarkar, J. Phys. Chem. A 107 (2003) 4973.
[72] C. Morell, A. Grand, A. Toro-Labbe, J. Phys. Chem. A 109 (2005) 205.
[73] E.D. Glendening, A.E. Reed, J.E. Carpenter, F. Weinhold, NBO Version 3.1, Theoretical Chemistry Institute and Department of Chemistry, University of Wisconsin, Madison, 1998.
[74] S. Larson, Chemical Physics, CRC Press, USA, 2012.
[75] A.S. El-Azab, Y.S. Mary, C.Y. Panicker, A.A.M. Abdel-Aziz, M.A. El-Sherbeny, C. Van Alsenoy, J. Mol. Struct. 1113 (2016) 133.
[76] N. Tewatia, A. Abida, K.P. Namdeo, J. Chem. Pharm. Res. 4 (2012) 1794.
[77] C. Sin, S. Lipinski, O. Gavrilova, K. Aden, A. Rehman, A. Till, A. Rittger, R. Podschum, U. Meyer-Hoftert, R. Haesler, E. Midtling, K. Putsep, M.A. McGuckin, S. Schreiber, S. Saftiq, P. Rosenstiel, Gut 62 (2013) 520.
[78] O. Trott, A.J. Olson, J. Comput. Chem. 31 (2010) 455.
[79] B. Kramer, M. Rarey, T. Lengauer, Proteins Struct. Funct. Genet. 37 (1999) 228.
[80] J. Zitko, B. Servusova, P. Paterova, J. Mandikova, V. Kubicek, R. Kucera, V. Hrabcova, J. Kunes, O. Soukup, M. Dolezal, Molecules 18 (2013) 14807.